

42	4.1 Event reconstruction	53
43	4.2 Event selection	55
44	4.3 Regions and channels	55
45	4.4 Data driven background simulation	55
46	5 The search for FCNC involving a top quark and a Z boson	57
47	5.1 Construction of template distributions	57
48	5.2 Systematic uncertainties	57
49	5.3 Limit setting procedure	57
50	5.4 Result and discussion	57
51	6 Conclusion and outlook	59
52	Bibliography	61

Experimental set-up

2

291 The main objective of the Large Hadron Collider (LHC) was the search for the Brout-Englert-
 292 Higgs boson. The Large Electron Positron (LEP) [45] and Tevatron [46] experiments had
 293 established that the mass of the scalar boson has to be larger than 114 GeV [47, 48], and smaller
 294 than approximate 1 TeV due to unitarity and perturbativity constraints [49]. On top of this,
 295 the search for new physics such as supersymmetry or the understanding of dark matter were
 296 part of the motivation for building the LHC. Since the start of its operation, the LHC is pushing
 297 the boundaries of the Standard Model, putting the most stringent limits on physics beyond the
 298 Standard Model as well as precision measurements of the parameters of the Standard Model. A
 299 milestone of the LHC is the discovery the scalar boson in 2012 by the two largest experiments
 300 at the LHC [7, 8].

301 This chapter is dedicated to the experimental set up of the LHC and the Compact Muon
 302 Solenoid (CMS) experiment. Section 2.1 describes the LHC and its acceleration process for
 303 protons to reach their design energies. The CMS experiment and its components are presented
 304 in Section 2.2. The upgrades performed during the long shutdown in 2013 are discussed
 305 in Section 2.2.4. The data acquisition of CMS is presented in Section 2.2.3, while the CMS
 306 computing model is shown in Section 2.2.5.

307 2.1 The Large Hadron Collider

308 The LHC has started its era of cutting edge science on 10 September 2008 [50] after approval by
 309 the European Organisation of Nuclear Research (CERN) in 1995 [51]. Installed in the previous
 310 LEP tunnels, the LHC consists of a 26.7 km ring, that is installed between 45 and 170 m under
 311 the French-Swiss border amidst Cessy (France) and Meyrin (Switzerland). Built to study rare
 312 physics phenomena at high energies, the LHC can accelerate two type of particles, protons or
 313 ions Pb^{45+} , and provides collisions at four interaction points, where the particle bunches are
 314 crossing. Experiments for studying the collisions are installed on each interaction point.

315 As can be seen in Figure 2.1, the LHC is last element in a chain that creates, injects and
 316 accelerates protons. The starting point is the ionisation of hydrogen, creating protons that are
 317 injected in a linear accelerator (LINAC 2). Here, the protons obtain an energy of 50 MeV. They
 318 continue to the proton synchrotron booster (PSB or Booster), where the packs of protons are

319 accelerated to 1.4 GeV and each pack is split up in twelve bunches with 25 ns spacing for Run 2
 320 (50 ns for Run 1). The proton synchrotron (PS) then increases their energy to 25 GeV before the
 321 super proton synchrotron (SPS) increases the proton energy up to 450 GeV. Each accelerator
 322 ring expands in radius in order to reduce the energy loss of the protons by synchrotron radiation¹
 323 Furthermore, the magnets responsible for the bending of the proton trajectories have to be
 324 strong enough to sustain to higher proton energy. Ultimately, the protons are injected into
 325 opposite directions into the LHC, where they are accelerated to 3.5 TeV (in 2010 and 2011),
 326 4 TeV (in 2012 and 2013) or 6.5 TeV (in 2015 and 2016) [52]. Before the start of the LHC
 327 in 2010, the previous energy record was held by the Tevatron collider at Fermilab, colliding
 328 proton with antiprotons at $\sqrt{s} = 1.96$ TeV. When completely filled, the LHC nominally contains
 2220 bunches in Run 2, compared to 1380 in Run 1 (design: 2200).

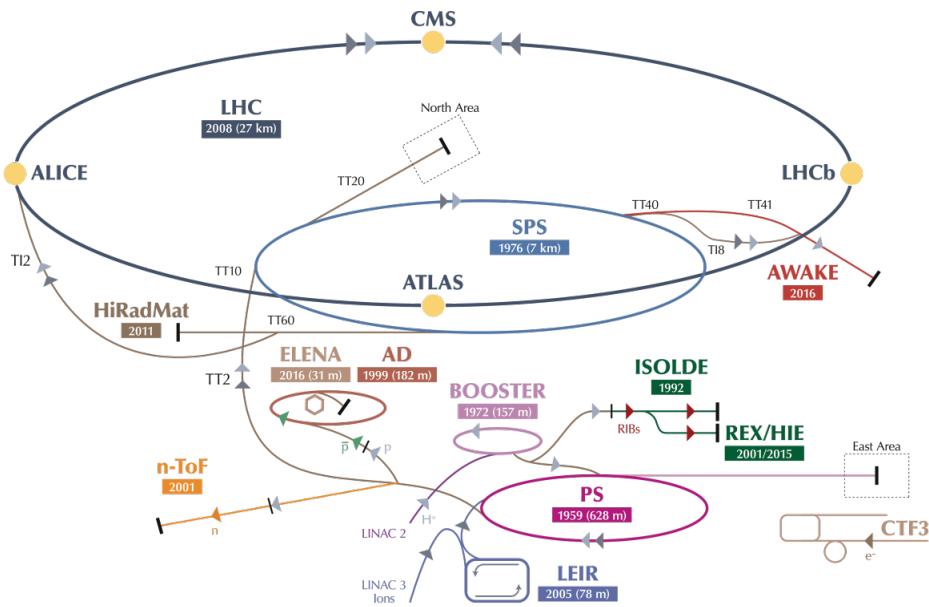


Figure 2.1: Schematic representation of the accelerator complex at CERN [53]. The LHC (dark blue) is the last element in chain of accelerators. Protons are successively accelerated by LINAC 2, the Booster, the Proton Synchrotron (PS) and the Super Proton Synchrotron (SPS) before entering the LHC.

329

330 Inside the LHC ring [54], the protons are accelerated by the means of radio frequency cavities,
 331 while 1232 dipole magnets of approximately 15 m long, each weighing 35 t ensure the deflection
 332 of the beams. The two proton beams circulate in opposite direction in separate pipes inside
 333 of the magnet. Through the use of a strong electric current in the coils around the beam pipe,
 334 magnetic fields are generated and cause the protons to bend in the required orbits. In order to
 335 get the coil to become superconducting and able to produce - with the aid of an iron return yoke
 336 - a strong magnetic field of 8.3 T, the magnet structure is surrounded by a vessel. This vessel is
 337 filled with liquid Helium making it possible to cool down the magnet to 1.9 K. In order to get

¹This energy loss is proportional to the fourth power of the proton energy and inversely proportional to the bending radius.

338 more focussed and stabilised proton beams, additional higher-order multipole and corrector
 339 magnets are placed along the LHC beam line.

340 The LHC is home to seven experiments, each located on an interaction point:

- 341 • A Toroidal LHC ApparatuS (ATLAS) [55] and the Compact Muon Solenoid (CMS) [56]
 342 experiments are the two general purpose detectors at the LHC. They both have a hermetic,
 343 cylindrical structure and were designed to search for new physics phenomena along with
 344 precision measurements of the Standard Model. The existence of two distinct experiments
 345 allows cross-confirmation of any discovery.
- 346 • A Large Ion Collider Experiment (ALICE) [57] and the LHC Beauty (LHCb) [58] exper-
 347 iments are focusing on specific phenomena. ALICE studies strongly interacting matter
 348 at extreme energy densities where a quark-gluon plasma forms in heavy ion collisions
 349 (Pb-Pb or p-Pb). LHCb searches for differences between matter and antimatter with the
 350 focus on b physics..
- 351 • The forward LHC (LHCf) [59] and the TOTal cross section, Elastic scattering and diffraction
 352 dissociation Measurement (TOTEM) [60] experiments are two smaller experiments that
 353 focus on head on collisions. LHCf consists of two parts placed before and after ATLAS
 354 and studies particles created at very small angles. TOTEM is placed in the same cavern as
 355 CMS and measures the total proton-proton cross section and studies elastic and diffractive
 356 scattering.
- 357 • The Monopoles and Exotics Detector At the LHC (MoEDAL) [61] experiment is situated
 358 near LHCb and tries to find magnetic monopoles.

For the enhancement of the exploration of rare events and thus enhancing the number of collisions, high beam energies as well as high beam intensities are required. The luminosity [62] is a measurement of the number of collisions that can be produced in a detector per square meter and per second and is the key role player in this enhancement. The LHC collisions create a number of events per second given by

$$N_{\text{event}} = L \sigma_{\text{event}}, \quad (2.1)$$

where σ_{event} is the cross section of the event of interest and L the machine luminosity. This luminosity depends only on the beam parameters and is for a Gaussian beam expressed as

$$L = \frac{1}{4\pi} N_b n_b f_{\text{rev}} \frac{N_b}{\epsilon_n} \left(1 + \left(\frac{\theta_c \sigma_z}{2\sigma^*} \right)^2 \right)^{-\frac{1}{2}} \frac{\gamma_r}{\beta^*}. \quad (2.2)$$

359 The number of particles per bunch is expressed by N_b , while n_b is the number of bunches
 360 per beam, f_{rev} the revolution frequency, γ_r the relativistic gamma factor, ϵ_n the normalized
 361 transverse beam emittance - a quality for the confinement of the beam , β^* the beta function at
 362 the collision point - a measurement for the width of the beam, θ_c the angle between two beams
 363 at the interaction point, σ_z the mean length of one bunch, and σ^* the mean height of one bunch.

364 In Equation 2.2, the blue part represents the stream of particles, the red part the brilliance, and
 365 the green part the geometric reduction factor due to the crossing angle at the interaction point.

366 The peak design luminosity for the LHC reached in 2016 is $10^{34} \text{ m}^{-2}\text{s}^{-1}$, which leads to about
 367 1 billion proton interactions per second. In 2016, the LHC was around 10% above this design
 368 luminosity [63]. The luminosity is not a constant in time since it diminishes due to collisions
 369 between the beams, and the interaction of the protons and the particle gas that is trapped in
 370 the centre of the vacuum tubes due to the magnetic field. The diffusion of the beam degrades
 371 the emittance and therefore also the luminosity. For this reason, the mean lifetime of a beam
 372 inside the LHC is around 15 h. The integrated luminosity - the luminosity provided in a certain
 373 time range - recorded by CMS and ATLAS over the year 2016 is given in Figure 2.2. In Run 2,
 the peak luminosity is $13\text{-}17 \cdot 10^{33} \text{ cm}^{-2}\text{s}^{-1}$ compared to $7.7 \cdot 10^{33} \text{ cm}^{-2}\text{s}^{-1}$ in Run 1.

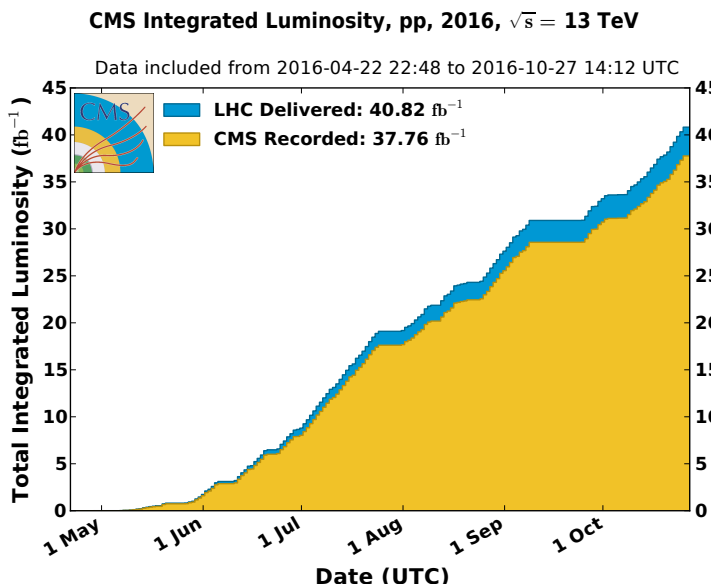


Figure 2.2: Cumulative offline luminosity measured versus day delivered to (blue), and recorded by CMS (orange) during stable beams and for proton collisions at 13 TeV centre-of-mass energy in 2016. The delivered luminosity accounts for the luminosity delivered from the start of stable beams until the LHC requests CMS to turn off the sensitive detectors to allow a beam dump or beam studies [64].

374

375 Multiple proton-proton interactions can occur during one bunch crossing, referred to as
 376 pileup. On average, the number of pileup events is proportional to the luminosity times the total
 377 inelastic proton-proton cross section. In 2016, an average of about 27 of pileup interactions
 378 has been observed in 13 TeV proton collisions at the interaction point of CMS. For 2012, this
 379 number was about 21 pileup interactions for 8 TeV collisions.

380 2.2 The Compact Muon Solenoid

381 At one of the collision points of the LHC, the CMS detector[65–67] is placed. Weighing 14 000 t,
 382 this cylindrical detector is about 28.7 m long and 15 m in diameter. It has an onion like structure

of several specialised detectors and contains a superconducting solenoid with a magnetic field of 3.8 T. Living in a hadronic environment, multi-jet processes produced by the strong interaction are a main source of background for rare physics processes. Therefore, good identification, momentum resolution, and charge determination of muons, electrons and photons are one of the main goals of the CMS detector. Additionally, a good charged particle momentum resolution and reconstruction efficiency in the inner tracker provides identification for jets coming from b quarks or tau particles can be identified. Also the electromagnetic resolution for an efficient photon and lepton isolation as well as a good hadronic calorimeter for the missing transverse energy² were kept into account while designing CMS. In Figure 2.3, an overview of the CMS detector is shown.

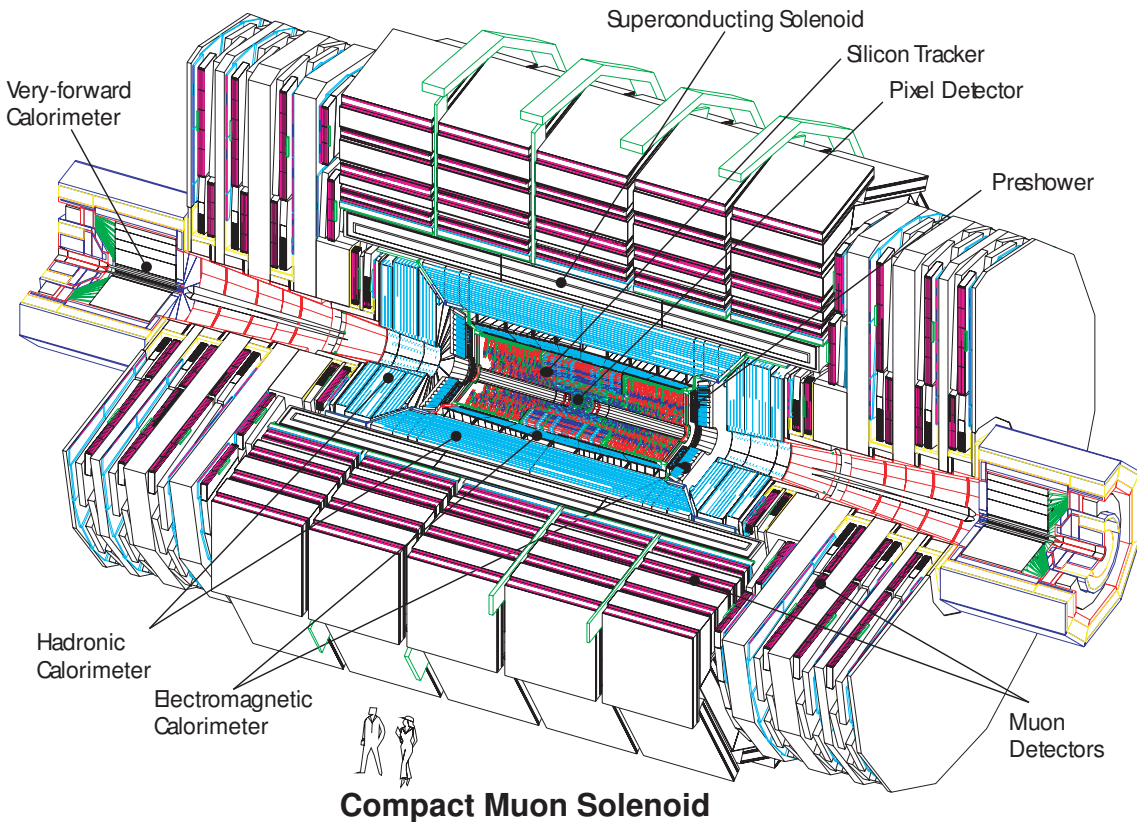


Figure 2.3: Mechanical layout of the CMS detector. Figure taken from [68].

392

393 2.2.1 CMS coordinate system

The coordinate system used by CMS can be found in Figure 2.4. The origin of the right handed orthogonal coordinate system is chosen to be the point of collisions. The x-axis points towards the centre of the LHC ring such that the y-axis points towards the sky, and the z-axis lies tangent to the beam axis. Since the experiment has a cylindrical shape, customary coordinates are used

²The missing transverse energy comes from an imbalance in the transverse plane. This will be discussed in Chapter 4.

to describe the momentum \vec{p} : the distance $p = |\vec{p}|$, the azimuthal angle³ $\phi \in [-\pi, \pi]$, the pseudo-rapidity⁴ η :

$$\eta = -\ln\left(\tan\left(\frac{\theta}{2}\right)\right). \quad (2.3)$$

For the energies considered at the LHC, where $E \gg m$, the pseudo-rapidity is a good approximation of the rapidity y

$$y = \frac{1}{2} \ln\left(\frac{E + p_z}{E - p_z}\right), \quad (2.4)$$

- ³⁹⁴ where the difference of rapidities of two particles is invariant under a Lorentz boost in the z-direction.

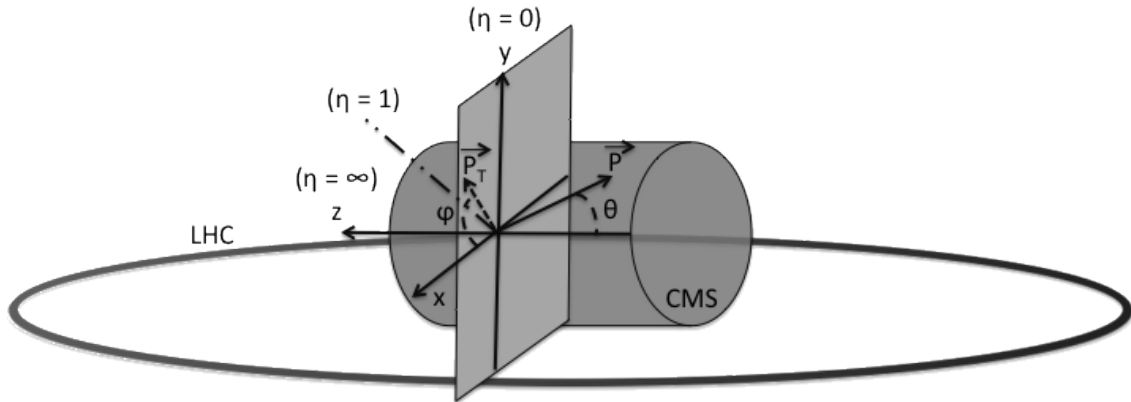


Figure 2.4: Representation of the coordinate system used by CMS. The point of origin is put at the collision point. The x-axis points towards the centre of the LHC ring such that the z-axis lies tangent to the beam axis.

- ³⁹⁵

396 2.2.2 Towards the heart of CMS

- ³⁹⁷ The CMS detector can be divided into two parts. A central barrel is placed around the beam
³⁹⁸ pipe ($|\eta| < 1.4$), and two plugs (end caps) ensure the hermeticity of the detector. In [Figure 2.3](#)
³⁹⁹ and [Figure 2.5](#) the onion like structure of the CMS detector is visible. The choice of a solenoid of
⁴⁰⁰ 12.9 m long and 5.9 m diameter gives the advantage of bending the particle trajectories in the
⁴⁰¹ transverse plane. The hadronic calorimeter ([Section 2.2.2.3](#)), the electromagnetic calorimeter
⁴⁰² ([Section 2.2.2.4](#)) and the tracker ([Section 2.2.2.5](#)) are within the solenoid ([Section 2.2.2.2](#)),
⁴⁰³ while the muon chambers ([Section 2.2.2.1](#)) are placed outside the solenoid. The data used for
⁴⁰⁴ the search presented in this thesis is collected after the long shutdown 1. After discussing each
⁴⁰⁵ part of CMS in their Run 1 configuration, [Section 2.2.4](#) elaborates on their different upgrades
⁴⁰⁶ for the data collected in Run 2.

³The azimuthal angle is the angle between the x-axis and the projection in the transverse plane of the momentum \vec{p} , denoted as \vec{p}_T .

⁴The pseudo rapidity is expressed by the polar angle θ between the direction of \vec{p} and the beam.

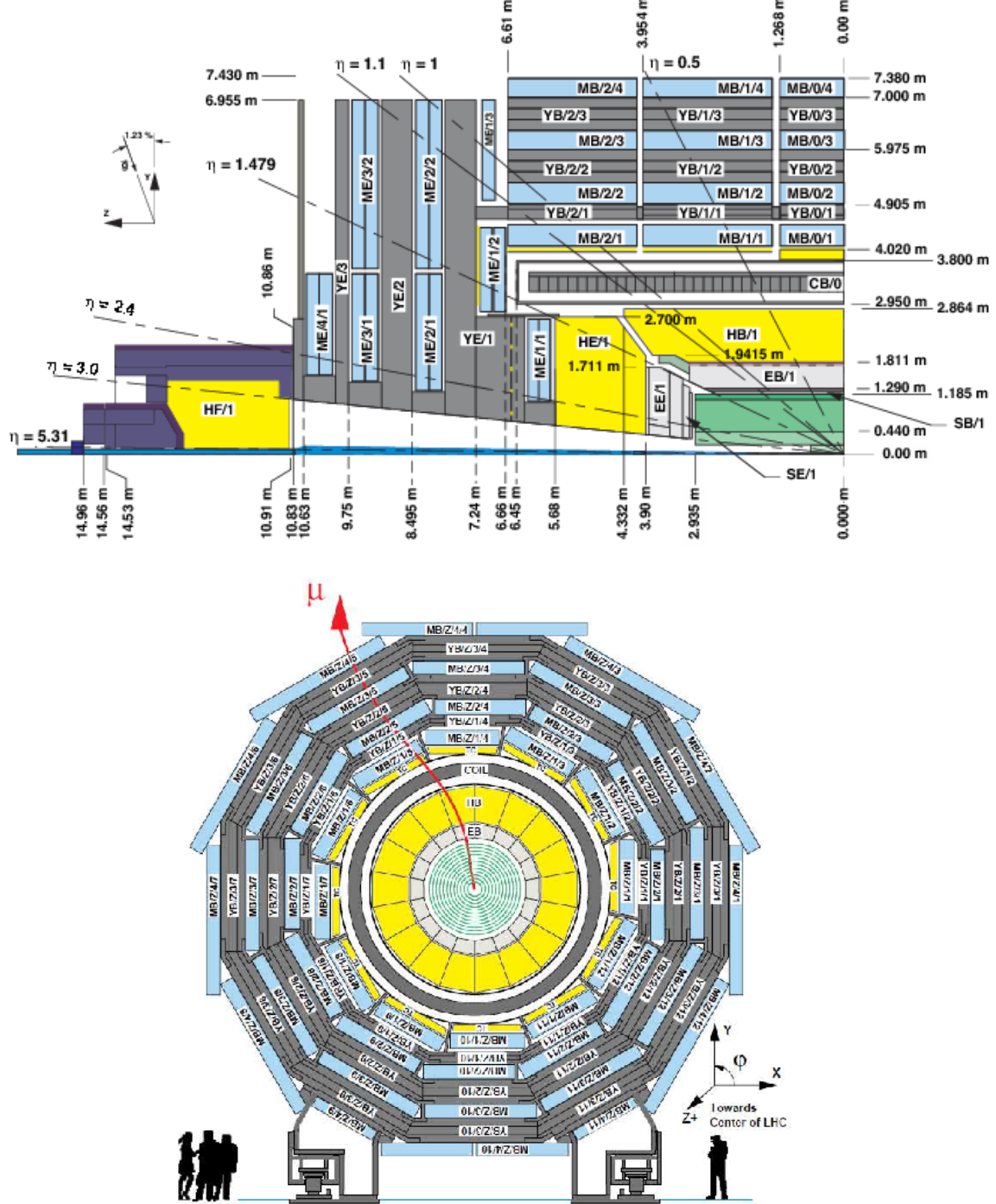


Figure 2.5: Schematic view of the CMS detector in the Run 1 configuration. The longitudinal view of one quarter of the detector is given on top, while the transversal view is shown on the bottom. The muon system barrel elements are denoted as $MBZ/N/S$, where $z = -2 \dots +2$ is the barrel wheel number, $n = 1 \dots 4$ the station number and $S = 1 \dots 12$ the sector number. Similarly, the steel return yokes are denoted as $YBZ/N/S$. The solenoid is denoted as $CB0$, while the hadronic calorimeter is denoted as HE (end cap)/ HB (barrel)/ HF (forward) and the electromagnetic calorimeter as EE (end cap)/ EB (barrel). The green part represents the tracking system (tracker + pixel). Figure taken from [69].

2.2.2.1 Muon system

The outermost part of CMS consists of the muon system. The magnet return yoke is interleaved with gaseous detector chambers for muon identification and momentum measurement. The barrel contains muon stations arranged in five separate iron wheels, while in the end cap four muon stations are mounted onto three independent iron discs on each side. Each barrel wheel has 12 sectors in the azimuthal angle.

The muon system is divided into three parts, shown in Figure 2.6. The muon rate and neutron induced backgrounds are small and the magnetic field is very low for the barrel, thus CMS can use drift tube (DT) chambers. For the end caps however, the muon and background flux is much higher and there is a need to use cathode strip chambers (CSC) which are able to provide a faster response, higher granularity and have a better resistance against radiation. In order to form a redundant trigger system, resistive plate chambers (RPC) are added. This makes a total of 250 DT, 540 CSC and 610 RPC chambers. In Figure 2.5 the arrangement is shown.

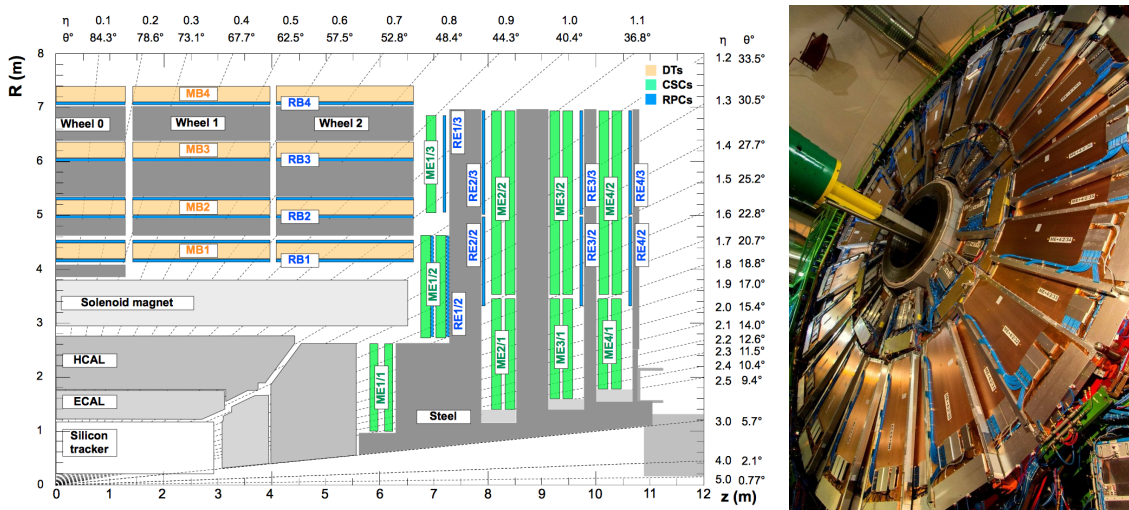


Figure 2.6: (Left) Schematic view of one quarter of the CMS muon system in the Run 1 configuration. The cathode strip chambers (CSC) are shown in green, the drift tubes (DT) are shown in yellow, while the resistive plate chambers (RPC) are shown in blue. Figure taken from [69]. (Right) Cathode strip chambers (ME+4/2 chambers on YE+3). Photo taken from [70].

419

Providing a measurement for $|\eta| < 1.2$, the DT chambers in the barrel are on average $2 \times 2.5 \text{ m}^2$ in size and consist of 12 layers of DT cells⁵ arranged in three groups of four. The $r\phi$ coordinate is provided by the two outside groups, while the middle group measures the z coordinate. For the outer muon station, the DT chambers contain only 8 layers of DT cells, providing a muon position in the $r\phi$ plane. There are four CSC stations in each end cap, providing muon measurements for $0.9 < |\eta| < 2.4$ (Run 1 configuration). These CSCs are multi-wired proportional chambers that consist of 6 anode wire planes crossed by 7 copper strips cathode panels in a gas volume. The r coordinate is provided by the copper strips, while the ϕ coordinate comes from the anode wires, giving a two dimensional position measurement. There are six

⁵The DT cells are 4 cm wide gas tubes with positively charged stretched wires inside.

429 layers of RPCs in the barrel muon system and one layer into each of the first three stations
 430 of the end cap. They are made from two high resistive plastic plates with an applied voltage
 431 and separated by a gas volume. Read out strips mounted on top of the plastic plates detect the
 432 signal generated by a muon passing through the gas volume. The RPCs provide a fast response
 433 with a time resolution of 1 ns and cover a range of $|\eta| < 1.8$ for the Run 1 configuration.

434 The muon system provides triggering on muons, identifying muons and improves the momen-
 435 tum measurement and charge determination of high p_T muons. On top of the muon system,
 436 the muon energy is deposited in the electromagnetic calorimeter, the hadronic calorimeter, and
 437 outer calorimeter. The high magnetic field enables an efficient first level trigger and allows a
 438 good momentum resolution of $\Delta p/p \approx 1\%$ for a p_T of 100 GeV and $\approx 10\%$ for a p_T of 1 TeV.
 439 There is an efficient muon measurement up to $|\eta| < 2.4$.

NOTE:
check numbers for run
2

440 2.2.2.2 Solenoid

441 Making use of the knowledge of previous experiments like ALEPH and DELPHI at LEP and H1
 442 at HERA, CMS choose for a large super conducting solenoid with a length of 12.9 m and a
 443 inner bore of 5.9 m [67]. With 2 168 turns, a current of 19.5 kA and a total energy of 2.7 GJ, a
 444 large bending power can be obtained for a modestly-sized solenoid. In order to ensure a good
 445 momentum resolution in the forward regions, a favourable length/radius was necessary. In
 446 [Figure 2.7](#), a photo of the CMS solenoid is shown.

447 The solenoid uses a high-purity aluminium stabilised conductor with indirect cooling from
 448 liquid helium, together with fully epoxy impregnation. A four-layer winding is implemented that
 449 can withstand an outward pressure of 64 atm. The NbTi cable is co-extruded by pure aluminium
 450 that acts as a thermal stabilizer and has an aluminium alloy for mechanical reinforcement. The
 451 return of the magnetic field is done by fives wheels, noted by YB in [Figure 2.5](#).

452 2.2.2.3 Hadronic calorimeter

453 The hadronic calorimeter (HCAL) is dedicated to precisely measure the energy of charged and
 454 neutral hadrons via a succession of absorbers and scintillators. This makes it crucial for physics
 455 analyses with hadronic jets or missing transverse energy. The HCAL barrel extends between
 456 $1.77 < r < 2.95$ m, where r is the radius in the transverse plane with respect to the beam. Due
 457 to space limitations, the HCAL needs to be as small as possible and is made from materials
 458 with short interaction lengths⁶. On top of this, the HCAL should be as hermetic as possible and
 459 extend to large absolute pseudo rapidities such that it can proved a good measurement of the
 460 missing transverse energy.

461 The quality of the energy measurements is dependent on the fraction of the hadronic shower
 462 that can be detected. Therefore, the HCAL barrel (HB) inside the solenoid is reinforced by an
 463 outer hadronic calorimeter between the solenoid and muon detectors (HO, see [Figure 2.8](#)),
 464 using the solenoid as extra absorber. This increases the thickness to 12 interaction lengths.

⁶Here the interaction length is the nuclear interaction length and this is the length needed for absorbing 36.7% of the relativistic charged particles. For the electromagnetic calorimeter this is defined in radiation length X_0 . The radiation length is the mean distance over which a high energy electron loses all but $1/e$ of its energy by bremsstrahlung.

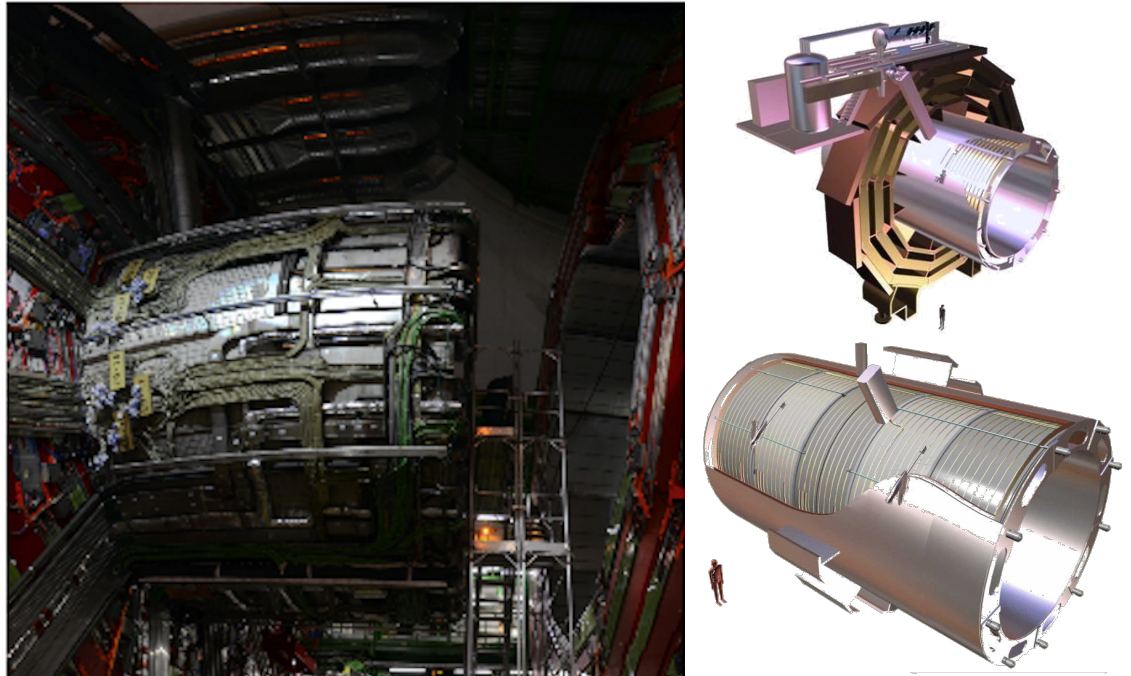


Figure 2.7: (Left) CMS solenoid during the long shutdown in 2013. (Right) An impression of the solenoid magnet taken from [71].

465 The HB and HO provide measurements for $|\eta| < 1.3$, while an end cap on each side (HE,
 466 $1.3 < |\eta| < 3$) and a forward calorimeter (HF, $3.0 < |\eta| < 5.2$) extend the pseudo rapidity
 467 range.

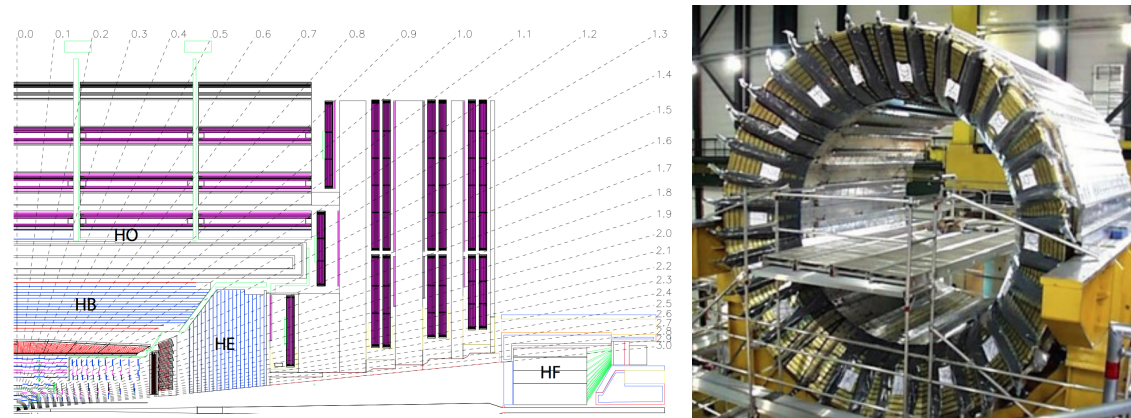


Figure 2.8: (Left) Longitudinal view of the CMS detector showing the locations of the HB, HE, HO, and HF calorimeters. Figure taken from [56]. (Right) CMS barrel calorimeter. Photo taken from [72].

468 The HB is made of 16 absorber plates where most of them are built from brass and others are
 469 made from stainless steel and is about five to ten interaction lengths thick. It is divided in $\eta \times \phi$
 470 towers and contains 2592 read out channels. The HO complements the HB and extends the
 471 reach up to twelve interaction lengths. This subsystem contains 2160 read out channels. The HE

472 is also composed of brass absorber plates and has a thickness corresponding to approximately
 473 ten interaction lengths, with 2592 read out channels.. The HF experiences intense particle
 474 fluxes with an expected energy of 760 GeV deposited on average in a proton interaction at a
 475 centre-of-mass of 14 TeV, compared to 100 GeV in the rest of the detector. Therefore, these are
 476 Cherenkov light detectors made of radiation hard quartz fibers. The main causes of such large
 477 energy events are high energy muons, cosmic particles and charged particles from late showering
 478 hadrons. During Run 1, it became clear that the glass windows of the photon multiplier tubes
 479 (PMTs) had to be replaced which was done during LS1 [73]. The HF represents 1728 read out
 480 channels.

481 The HCAL and electromagnetic calorimeter combined can measure the hadron energy with a
 482 resolution $\Delta E/E \approx 100\% \sqrt{E[\text{GeV}]} + 5\%$.

483 2.2.2.4 Electromagnetic calorimeter

484 The electromagnetic calorimeter (ECAL) is designed to measure the energy of photons and
 485 electrons and covers $|\eta| < 3$. It is an hermetic, homogeneous detector and consists of 75 848
 486 lead tungstate (PbWO_4) crystals. These crystals have a fast response time - 80% of the light
 487 is emitted within 25 ns - and are radiation hard. The electromagnetic showers produced by
 488 passing electrons or photons ionize the crystal atoms which emit a blue-green scintillation light,
 489 that is collected by silicon avalanche photodiodes (APDs) in the barrel and vacuum phototriodes
 490 (VPTs) in the end caps. The crystals and the APD response is sensitive to temperature changes
 491 and require a stable temperature.

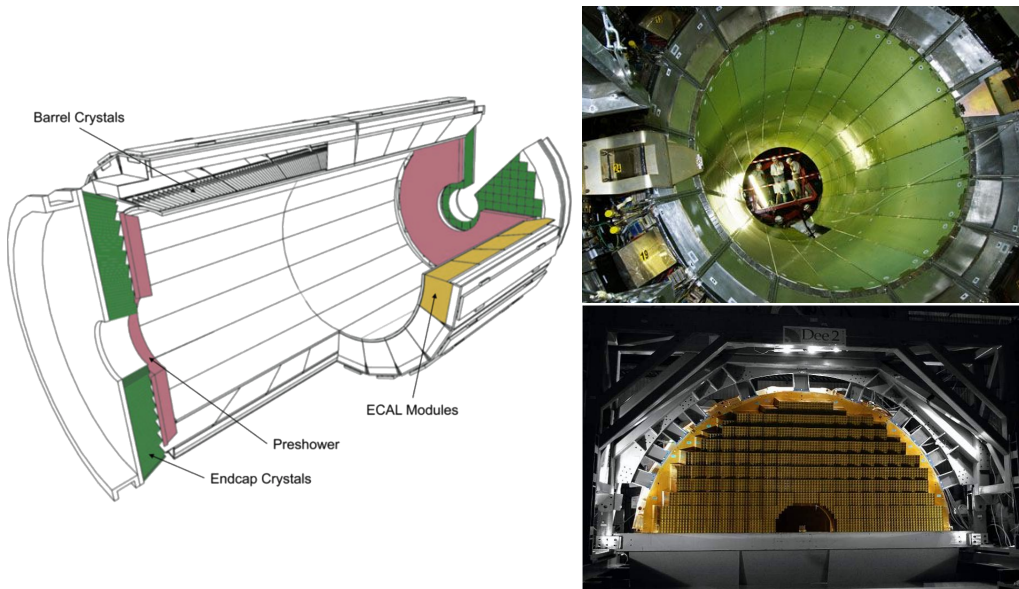


Figure 2.9: (Left) Schematic cross section of the electromagnetic calorimeter taken from [56]. (Right top) The ECAL barrel during construction [74]. (Right bottom) One half of an EE [75].

492 There are three regions: a central barrel (EB), an endcap region (EE) and a preshower (ES)
 493 (Figure 2.9). The EB has an inner radius of 129 cm and corresponds to a pseudo rapidity of $0 <$
 494 $|\eta| < 1.479$. At a distance of 314 cm from the vertex and covering a pseudo rapidity of $1.479 <$

495 $|\eta| < 3.0$, are the EE. They consist of semi-circular aluminium plates from which structural
 496 units of 5×5 crystals (super crystals) are supported. The ES is placed in front of the crystal
 497 calorimeter over the end cap pseudo rapidity range with two planes of silicon strip detectors as
 498 active elements.

The electromagnetic shower will typically involve more than one channel. More than 90% of the energy of a 35 GeV electron or photon is contained in a 5×5 matrix of crystals. Therefore, a clustering algorithm is performed in order to associate the energy deposits to the particles impinging the calorimeter. The achieved precision [76] for the barrel is 2.10^{-3} rad in ϕ and 10^{-3} in η . For the end caps this is 5.10^{-3} rad in ϕ and 2.10^{-3} in η . The energy is reconstructed by a supercluster algorithm, taking into account energy radiated via bremsstrahlung or conversion [56]. The energy resolution is given by

$$\frac{\sigma(E)}{E} = \frac{2.8\%}{\sqrt{E}} \oplus \frac{0.128}{E(GeV)} \oplus 0.3\%, \quad (2.5)$$

499 in the absence of a magnetic field, where the contributions come from the stochastic, noise and
 500 constant terms respectively. The dominating term is the constant term ($E_{shower} \approx 100$ GeV)
 501 and thus the performance is highly dependent on the quality of calibration and monitoring .

502 2.2.2.5 Inner tracking system and operations

503 The tracking system (tracker) [77] is the detecting unit closest to the point of interaction.
 504 Responsible for the reconstruction of trajectories from charged particles with $|\eta| < 2.5$ that are
 505 bent by the magnetic field, it provides a measurement of the momentum. The tracker is also
 506 responsible for the determination of the interaction point or vertex. It should be able to provide
 507 high granularity as well as fast read out, and be able to endure high radiation. For this reason,
 508 the CMS collaboration choose silicon detector technology.

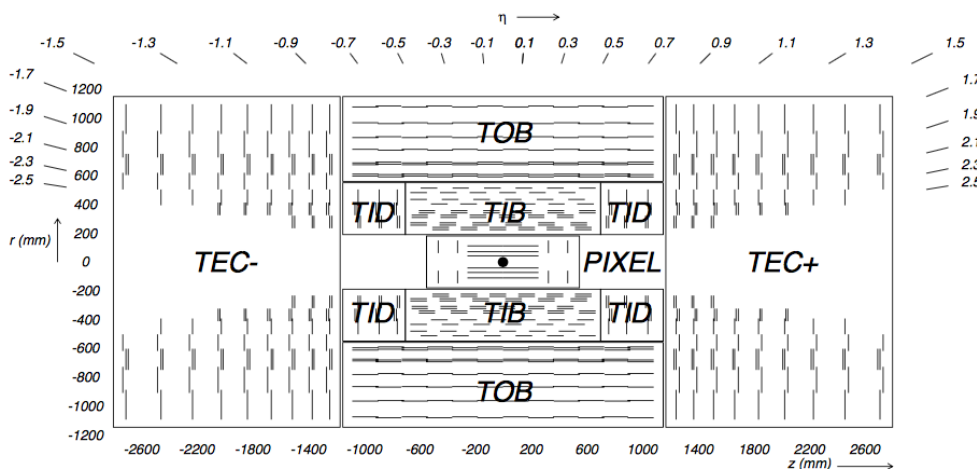


Figure 2.10: Schematic cross section through the CMS tracker. Each line represents a detector module. Double lines indicate back-to-back modules that deliver stereo hits. Figure taken from [56].

509 The tracking system consists of a cylinder of 5.8 m long and 2.5 m in diameter. It is immersed
 510 in a co-axial magnetic field of 3.8 T provided by the solenoid. As shown in Figure 2.10, the

511 tracker is built up from a large silicon strip tracker with a small silicon pixel tracker inside. The
 512 inner pixel region ($4.4 < r < 10.2$ cm), gets the highest flux of particles. Therefore, pixel silicon
 513 sensors of $100 \times 150 \mu\text{m}^2$ are used. It consists of three cylindrical barrels that are complemented
 514 by two discs of pixel modules at each side. The silicon strip tracker ($20 < r < 116$ cm) has three
 515 subdivisions. The Tracker Inner Barrel and Discs (TIB, TID, see Figure 2.12) are composed
 516 of four barrel layers accompanied by three discs at each end. The outer part of the tracker -
 517 Tracker Outer Barrel (TOB) - consists of 6 barrel layers. In the outer discs, there are nine discs
 518 of silicon sensors, referred to as Tracker End Caps (TEC).



Figure 2.11: The pixel barrel being re-installed after the Long Shutdown in 2015, around the beam pipe at CMS [78].



Figure 2.12: First half of the inner tracker barrel, consisting of three layers of silicon modules [79].

519 The pixel, shown in Figure 2.11, has 1440 modules that cover an area of about 1 m^2 and have
 520 66 million pixels. It provides a three-dimensional position measurement of the hits arising from
 521 the interaction from charged particles with the sensors. In transverse coordinate ($r\phi$), the hit
 522 position resolution is about $10 \mu\text{m}$, while $20\text{-}40 \mu\text{m}$ is obtained in the longitudinal coordinate
 523 (z). The sensor plane position provides the third coordinate. The TIB/TID, shown in Figure
 524 2.12, delivers up to four $r\phi$ -measurements using a $320 \mu\text{m}$ thick silicon micro-strip sensors.
 525 These sensors are placed with their strips parallel to the beam axis in the barrel and radial
 526 in the discs. In the TIB, the first two layers have a strip pitch of $80 \mu\text{m}$, while the remaining
 527 to have a strip pitch of $120 \mu\text{m}$. This leads to a respective single point resolution of $23 \mu\text{m}$
 528 and $35 \mu\text{m}$. For the TID, the pitch varies between $100 \mu\text{m}$ and $141 \mu\text{m}$. The TOB provides six
 529 $r\phi$ -measurements with a single point resolutions of $53 \mu\text{m}$ in the first four layers, and $35 \mu\text{m}$ in
 530 the last two layers. It consists of $500 \mu\text{m}$ thick micor strip sensors with strip pitches of $183 \mu\text{m}$
 531 (first 4 layers) or $122 \mu\text{m}$ (last two layers). The TEC provides up to 9 ϕ -measurements via 9
 532 discs consisting of up to 7 rings of silicon microstrip sensor of $97 \mu\text{m}$ to $184 \mu\text{m}$ average pitch.

533 A second co-ordinate measurement (z in the barrel, r on the discs) is provided through the
 534 use of a second micro strip detector module mounted back-to-back with a stereo angle of 100
 535 mrad. This is done on the modules in the first two layers and rigns of the TIB, TID, and TOB, as
 536 wel as rigns 1,2, and 5 of the TECs (blue line in Figure 2.10). The resolution in the z direction is
 537 approximately $230 \mu\text{m}$ in the TIB and $530 \mu\text{m}$ in the TOB, and is varying with pitch in the TID
 538 and TEC. To allow overlay and avoid gaps in acceptance, each module is shifted slightly in r or
 539 z with respect to its neighbouring modules within a layer. With this detector lay out, at least
 540 nine points per charged particle trajectory can be measured in an $|\eta|$ range up to 2.4, where at
 541 least four of them being two dimensional. The CMS silicon tracker provides 9.3 million readout

542 channels and covers an active area of about 198 m^2 .

543 2.2.3 Data acquisition

544 At a design luminosity of $10^{34} \text{ m}^{-2}\text{s}^{-1}$, the proton interaction rate exceeds 1 GHz. Given the
 545 large size of an event (about 1 MB), the high crossing rate, and that typically tens of collisions
 546 happen at the same time, it is impossible for the CMS experiment to store all the data generated.
 547 In order to deal with the large amount of data, a two level trigger system has been put in place.
 548 The first level (Level-1) is a custom hardware system, while a second high level trigger (HLT) is
 549 software based running on a large farm of computers.

550 CMS Level-1 Trigger

551 The Level-1 Trigger has to be a flexible, maintainable system, capable of adapting to the
 552 evolving physics programme of CMS [80]. Its output rate is restricted to 100 kHz imposed
 553 by the CMS readout electronics. It is implemented by custom hardware and selects events
 554 containing candidate objects - e.g. ionization deposits consistent with a muon, or energy clusters
 555 corresponding to an electron / photon / tau lepton / missing transverse energy / jet. Collisions
 556 with large momenta can be selected by using scalar sum of the transverse momenta of the jets.

557 By buffering the raw data from the CMS subdetectors in front-end drivers, the Level-1 Trigger
 558 has a pipeline memory of 3.2 μs to decide whether to keep an event or reject it. The trigger
 559 primitives (TP) from the calorimeters and muon detectors are processed in several steps and
 560 combined into a global trigger. This information is then combined with the input from the other
 561 subsystems for the HLT. The separate inputs are synchronized to each other and the LHC orbit
 562 clock and sent to the global trigger module. Here, Level-1 Trigger algorithms are performed
 563 within 1 μs to decide whether to keep the event.

564 CMS HLT Trigger

565 The HLT is an array of commercially available computers with a programmable menu that has
 566 an output rate of on average 400 Hz for off-line event storage. The data processing is based on
 567 an HLT path. This is a set of algorithmic steps to reconstruct objects to define selection criteria.
 568 Here, the information of all subdetectors can be used to perform algorithms on higher level
 569 reconstructed objects.

570 2.2.4 Phase 1 upgrades

571 Before the start of taking collision data for 13 TeV operations on 3 June 2015, CMS had a long
 572 shutdown (LS1) [81]. During this shutdown, the section of the beryllium beam pipe within CMS
 573 was replaced by a narrower one. This operation required the pixel to be removed and reinserted
 574 into CMS. In Run 2, higher particle fluxes with respect to Run 1 are expected. To avoid long
 575 damage caused by the intense particle flux at the heart of CMS, the tracker is been made ready
 576 to operate at much lower temperature than during Run 1. The electromagnetic calorimeter
 577 preshower system had been damaged during Run 1, therefore the preshower discs were removed,
 578 repaired and reinstalled successfully inside CMS in 2014. To help the discrimination between
 579 interesting low momentum muons coming from collisions and muons caused by backgrounds, a

580 fourth triggering and measurement station for muons was added in each of the end caps. Several
 581 new detectors were installed into CMS for measuring the collision rate within the detector and
 582 monitors beam related backgrounds.

583 During the LS1, the muon system underwent major upgrades [82, 83]. In the fourth station
 584 of each end cap, the outermost rings of CSC and RPC chambers were completed, providing an
 585 angular coverage of $1.2 < |\eta| < 1.8$ for Run 2, increasing the system redundancy, and allowing
 586 tighter cuts on the trigger quality. In order to reduce the environmental noise, outer yoke discs
 587 have been placed on both sides for the end caps. At the innermost rings of the first station,
 588 the CSCs have been upgraded by refurbishing the readout electronics to make use of the full
 589 detector granularity instead of groups of three as was the case for Run 1. In Figure 2.6 (right),
 590 the refurbishing of the CSCs is shown.

591 Since the HF experiences intense particle fluxes, it became clear during Run 1 that the glass
 592 windows of the PMTs need replacing. For the ECAL in Run 1, the energy reconstruction happened
 593 via a weighted sum of the digitized samples [84]. For Run 2 however, the reconstruction had
 594 to be made more resistant for out of time pile up and a multi-fit approach has been set into
 595 place. In this approach, the pulse shape is modelled as a sum of one in-time pulse plus the out
 596 of time pulses [76]. The energy resolution is better than 2% in the central barrel region and
 597 2-5 % elsewhere.

During the first data taking period of the LHC (2010 to 2013), the tracker operated at $+4^\circ\text{C}$. With the higher LHC beam intensities from 2015 onwards, the tracker needs to be operated at much lower temperatures. The reason for this is that with intense irradiation, the doping concentration changes, the leakage current increases proportional to the fluence and the charge collection efficiency decreases due to charge trapping. Mostly the leakage current (I) is affected by the temperature change:

$$I \propto T^2 e^{-\frac{E_g}{2kT}}, \quad (2.6)$$

598 where T is the operating temperature, E_g the band gap and k the Boltzmann constant. There is
 599 approximately a factor 15 between the leakage currents at room temperatures and at -10°C .

600 During the LS1, the CMS cooling plant was refurbished [85] and the fluorocarbon cooling
 601 system overhauled. To help to suppress the humidity inside the tracker, new methods for vapour
 602 sealing and insulation were applied. Furthermore, several hundred high-precision sensors are
 603 used to monitor the humidity and temperature. In order to get as dry air as possible, a new
 604 dry-gas plant provides eight times more dry gas (air or nitrogen) than during the first run, and
 605 allows regulation of the flow. As a final addition, the cooling bundles outside the tracker are
 606 equipped with heater wires and temperature sensors in order to maintain safe operations above
 607 the cavern dew point. For the data taking in 2015-2016, the tracker operated at -15°C .

608 In Run 2, with the increase in centre of mass energy and a higher luminosity, a larger number
 609 of simultaneous inelastic collisions per crossing is expected with respect to Run 1. For this, the
 610 CMS Level-1 has been upgraded [86]. All hardware, software, databases and the timing control
 611 system have been replaced for Run 2, where the main changes are that the muon system now
 612 uses the redundancy of the muon detector system earlier to make a high resolution muon trigger.

613 Other upgrades are that the calorimeter system isn't bound any more for streaming data and
614 the global trigger has more Level-1 Trigger algorithms.

615 After the first half of Run 2, the innermost part of detection material in CMS (pixel) was
616 upgraded by adding a fourth layer , enhancing the particle tracking capabilities of CMS. The
617 data used in the framework of this thesis however is from before this upgrade. More information
618 on the Pixel upgrade can be found in Refs. [87, 88].

619 **2.2.5 CMS computing model**

620 The selected data is stored, processed and dispersed via the Worldwide Large Hadron Collider
621 GRID (WLCG) [89, 90]. This has a tiered structure that functions as a single, coherent system.

622 At CERN and the Wigner Research Center for physics, a single Tier-0 is located. The raw data
623 collected by CMS is archived here, and a first reconstruction of the data is done. This data is
624 then already in a file format usable for physics analysis. Furthermore, it is able to reprocess
625 data when new calibrations become available. The Tier-0 site distributes this data to a total of
626 14 Tier-1 centres. They carry out data reprocessing and store real data as well as simulated
627 data. The Tier-1 further distributes the data to over 150 Tier-2 centres. These make the data
628 accessible for physics analysis and are also being used for the production of simulated data. The
629 data is made accessible for physicists around the world.

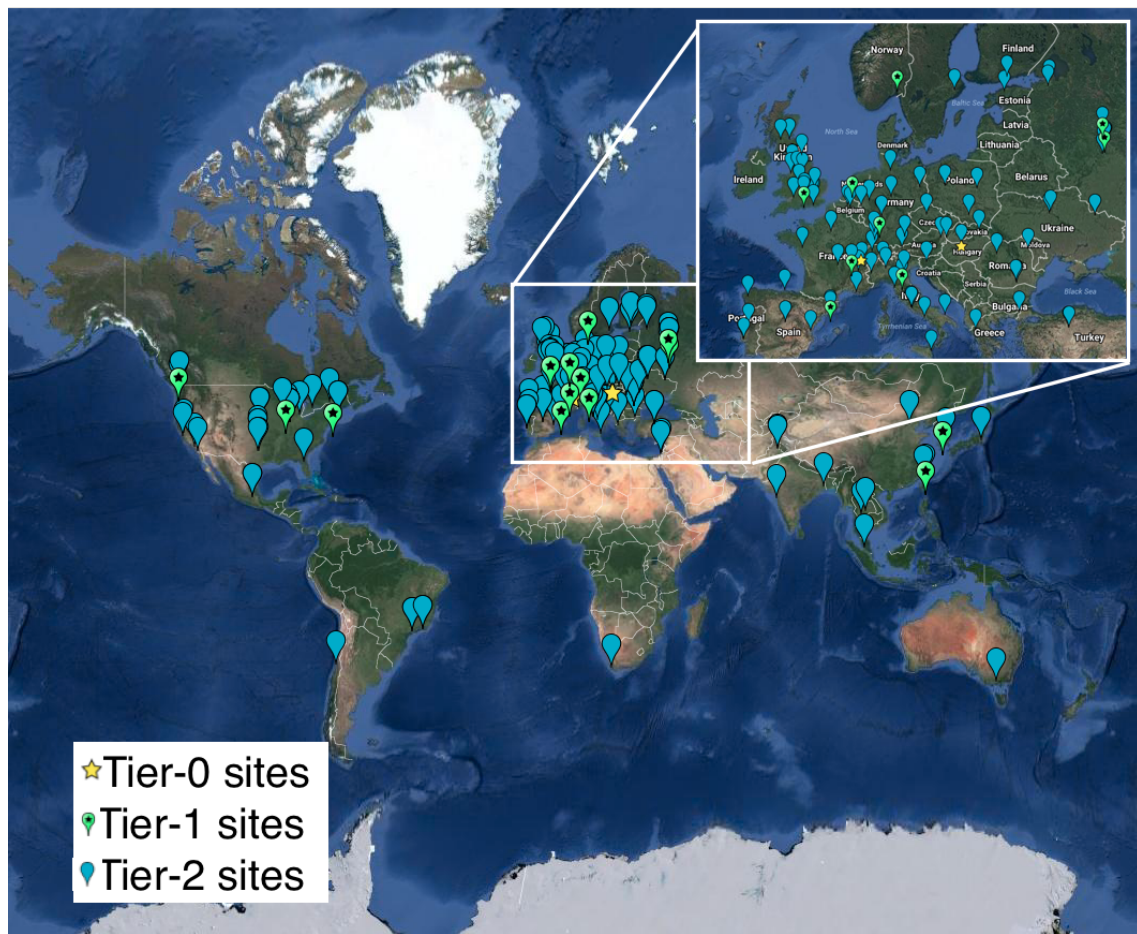


Figure 2.13: Worldwide LHC Computing Grid in 2017 [91].

